J. Fluid Mech. (1993), *vol.* 253, *pp.* 45–65

Interannual planetary wave breaking in the presence of Ekman pumping and mean flow

By ZHENGYU LIU†
Joint Program of MIT/Woods Hole Oceanographic Institution

(Received 5 December 1991 and in revised form 5 February 1993)

A two-layer planetary geostrophic model is adopted to study the breaking of planetary waves in the presence of Ekman pumping and the associated mean flow. The governing equation for the interface is a quasi-linear equation, which is solved analytically by the method of characteristics. The waves are forced by annual or interannual upwelling or downwelling along the eastern boundary of a subtropical gyre. It is found that the time and position at which breaking occurs is mainly determined by the speed and depth of the eastern boundary perturbation, while the intensity of a breaking front is mainly determined by the amplitude of the perturbation. The breaking of a planetary wave is affected significantly by Ekman pumping and the associated mean flow, particularly for annual and interannual forcing. Downward Ekman pumping, as in a subtropical gyre, suppresses breaking in downwelling waves caused by eastern boundary downwelling, but enhances breaking in upwelling waves caused by eastern boundary upwelling. In the presence of steady downward Ekman pumping, downwelling breaking will not occur except for interfaces near the surface. The structure and intensity of a breaking front is also discussed.

1. Introduction

Observations have shown the existence of basin-scale fronts: the Subarctic Front and Subtropical Front in the North Pacific are two examples (Roden 1976, 1980; Levine & White 1981). There is also evidence of large-scale frontal structures and baroclinic jets in the North Atlantic (McWilliams *et al.* 1983; Hua, McWilliams & Owens 1986). Vertically, some of the large-scale fronts can extend through the main thermocline. Some theories have been proposed to explain these basin-scale fronts (Roden 1976, 1980; Cushman-Roisin 1984; Dewar 1991).

Although these fronts seem to possess clear time-mean frontal structures, more detailed observations indicate that each has strong temporal variability and finer frontal structures (Niiler & Reynolds 1984). To date, the physical mechanisms for this finer structure and temporal variability are not well understood. Here, it is suggested that the breaking of planetary waves is one important mechanism, because breaking can create large-scale density frontal structures and thermal wind jets in the ocean. Here, we will explore the wave breaking with the emphasis on the effect of Ekman pumping and the associated mean flows.

Planetary wave breaking was first studied by Anderson & Killworth (1979). Using a $1\frac{1}{2}$ layer model, they demonstrated that for annual upwelling and downwelling at the eastern boundary, a planetary wave breaks soon after it leaves the eastern boundary. Dewar (1987) studied the breaking of free planetary waves in a two-layer model. In

† Present address: PO Box CN710, Sayre Hall, Princeton University, Princeton, NJ08544-0710, USA.

these two works, the thermocline structure and circulation are simple: Anderson & Killworth have one-dimensional thermocline structure, and Dewar's analysis, there are no mean Ekman pumping and flows. Here, we will study further the breaking of planetary waves in the presence of Ekman pumping and its associated two-dimensional mean flow. The main difficulty lies in both the mean flow field and the two-dimensional structure. There is no general theory dealing with temporal two-dimensional fronts. For simplicity, we only consider the breaking of waves forced by upwelling and downwelling at the eastern boundary which may be caused by either an alongshore wind variation or a coastal Kelvin wave coming from the equator. We hope that the results may shed light on the more general case of the breaking of planetary waves forced by other mechanisms such as a local wind or buoyancy flux anomalies in other parts of the ocean.

We will study the breaking of two types of disturbances: a downwelling wave which is caused by lowering the interface at the eastern boundary, and an upwelling wave which is forced by lifting the interface. Since deepening the interface at the eastern boundary causes the interface to shoal towards the west, producing a northward thermal wind, it is intuitively expected that the breaking of a deepening wave front will be accompanied by a northward thermal wind jet. Similarly, a shallowing breaking front is accompanied by a southward thermal wind jet.

The work is arranged as follows. A two-layer planetary geostrophic model is developed in §2. The interface is governed by a quasi-linear equation and is solved analytically by the method of characteristics. In §3, we review and further explore the breaking of a free wave, which is generated in the absence of mean Ekman pumping. From analytical solutions, it is possible to calculate the time and position where breaking first occurs. In addition, the discussion of the breaking of the free wave will help us to understand the cases with Ekman pumping and the associated mean circulation presented in §4, which represents the core material of the paper. It will be found that the breaking time, position and the intensity of the breaking front will be changed substantially by the Ekman pumping and mean flow.

2. The model and solution

2.1. *The model*

The model is a two-layer, planetary geostrophic one with a rigid flat bottom, and schematic view of the three-dimensional geometry is depicted in figure 1. The densities of the upper and lower layers are represented by ρ_1 and ρ_2 respectively. The thickness of the upper layer is h while the total depth is H. Ekman pumping w_e is imposed at the surface. The northern and southern boundaries of the subtropical gyre, defined to be where Ekman pumping vanishes, are located at the latitudes with the Coriolis parameters f_n and f_s, respectively. The eastern and western boundaries are set at $x_e = 0$ and $x_w < 0$. A rigid and flat bottom $H =$ constant is used, though we should point out, in connection with application to the real ocean, that we imagine, the bottom of the model ocean to be the bottom of the main thermocline, or the depth to which the wind-driven gyre penetrates. This imaginary bottom is neither rigid nor flat in the real ocean.

For a gyre-scale circulation, the hydrostatic balance yields the dynamic pressures in both layers as

$$p_1 = \rho_0 \gamma \eta, \quad p_2 = \rho_0 \gamma(\eta - h). \tag{2.1a}$$

Here, ρ_0 is the mean density and $\gamma = g(\rho_2 - \rho_1)/\rho_0$ is the reduced gravity; η is the elevation equivalent to an upper-layer pressure such that $\gamma\eta = \rho_0(p_{\text{surface}} + g\xi)$, where

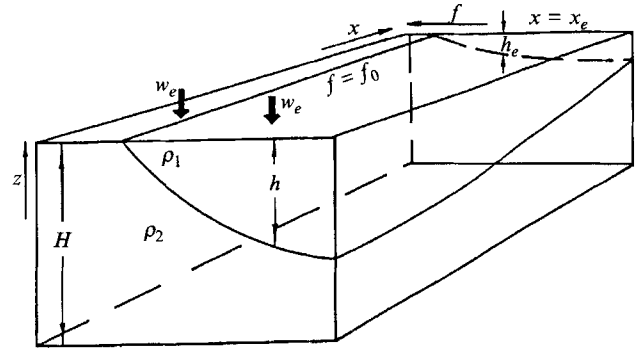

FIGURE 1. A three-dimensional view of the geometry of the model.

ξ is the surface elevation. Implicitly, it has been assumed that $(\rho_2-\rho_1)/\rho_0 \ll 1$. Using the planetary geostrophic approximation, the momentum equations are simply the geostrophic balance in each layer:

$$v_n = p_{nx}/\rho_0 f, \quad u_n = -p_{ny}/\rho_0 f, \quad n = 1,2, \tag{2.1b}$$

where $n = 1$ refers to the upper layer and $n = 2$ to the lower layer. In addition, we have the Sverdrup relation and the conservation of the lower-layer potential vorticity $q = f/(H-h)$ respectively:

$$\beta[v_1 h + v_2(H-h)] = f w_e, \tag{2.1c}$$

$$(\partial_t + \boldsymbol{v}_2 \cdot \nabla) q = 0. \tag{2.1d}$$

Using (2.1*a*, *b*), the Sverdrup relation (2.1*c*) can be integrated explicitly to give

$$2H\eta + (H-h)^2 = D^2 + 2H\eta_e + (H-h_e)^2, \tag{2.2a}$$

where

$$D^2 = \frac{2f^2}{\beta\gamma}\int_0^x w_e(x,f,t)\,\mathrm{d}x; \quad \eta_e(f,t) = \eta|_{x=0}, \quad h_e(f,t) = h|_{x=0}. \tag{2.2b}$$

Here, η_e and h_e are respectively the upper-layer pressure and interface depth at the eastern boundary. Therefore, we can derive the lower-layer pressure in (2.1*a*) as

$$p_2 \sim \eta - h = \frac{D^2-(H^2+h^2)}{2H} + \eta_e + \frac{(H-h_e)^2}{2H}. \tag{2.3}$$

Substituting (2.3) into (2.1*b*) yields the velocity in layer 2 (u_2, v_2). Then, substituting the velocity into (2.1*d*), we obtain the equation for the interface as

$$h_t + v_B h_f + [u_B + C(h)]\, h_x = -(1-h/H)\, w_e, \tag{2.4a}$$

where a flat bottom H = constant has been used and the y-coordinate is changed to the Coriolis parameter f by using $\mathrm{d}f = \beta\,\mathrm{d}y$. In addition, u_B, $v_B(\equiv \mathrm{d}f/\mathrm{d}t)$ and $C(h)$ are the barotropic velocities and the phase speed of the non-dispersive Rossby wave, respectively,

$$\left.\begin{aligned} (u_B, v_B) \equiv \frac{h\boldsymbol{v}_1 + (H-h)\,\boldsymbol{v}_2}{H} &= \left[-\frac{\left(f^2\int_0^x w_e\,\mathrm{d}x\right)_f}{Hf} + u_{BE}, \quad \frac{f w_e}{H}\right], \\ C(h) &= -\frac{\beta\gamma h(H-h)}{f^2 H}. \end{aligned}\right\} \tag{2.4b}$$

Here u_{BE} is the barotropic velocity at the eastern boundary, which hereafter will be assumed zero, i.e.

$$u_{BE} = \left[\eta_e + \frac{(H-h_e)^2}{2H}\right]_y = 0. \tag{2.4c}$$

Since the barotropic flow in (2.4*a*) is completely determined by the Sverdrup relation as shown in (2.4*b*), the evolution equation (2.4*a*) is quasi-linear. The characteristics are simply the ray paths of baroclinic planetary waves in the presence of a barotropic flow. This equation has previously been derived by Rhines (1986) and Dewar (1987).

We non-dimensionalize the evolution equation (2.4*a*). Denoting a dimensional quantity by a superscript asterisk, we have the non-dimensional quantities

$$f = f^*/f_n, \quad \beta = \beta^*/\beta_0, \quad t = t^*/T_W, \quad x = x^*/L, \quad h = h^*/H, \quad w = w^*/W. \tag{2.5}$$

In (2.5), W, f_n, β_0, H represent respectively the typical Ekman pumping velocity, the Coriolis parameter at the northern boundary of the subtropical gyre, the mean β-value in a subtropical gyre and the total depth. In addition, $T_W = H/W$, $\gamma = 2\ \mathrm{cm\ s^{-2}}$, $L = C_{\beta H} T_W$, and $C_{\beta H} = \beta_0 L_D^2$, $L_D^2 = \gamma H/f_n^2$ with L_D and $C_{\beta H}$ being the deformation radius and the typical mid-latitude Rossby wave speed. T_W is then the advective timescale for a particle to sink to the bottom of the main thermocline and L is the zonal scale across which a mid-latitude planetary wave travels in one advective timescale. If we choose the parameters as $W = 10^{-4}$ cm/s, $f_n = 2\Omega \sin(45°) = 10^{-4}\ \mathrm{s^{-1}}$, $H = 600$ m, $\beta_0 = (2\Omega/a)\cos(35°) = 1.87 \times 10^{-13}\ \mathrm{s^{-1}\ cm^{-1}}$, it follows that $T_W \approx 20$ years, $L \approx 8400$ km, $C_{\beta H} \approx 1.6\ \mathrm{cm\ s^{-1}}$, $L_D \approx 33$ km. With (2.4*c*) and (2.5), the baroclinic evolution equations (2.4*a*, *b*) become

$$h_t + \boldsymbol{v}_B \cdot \nabla h + C(h)\, h_x = -(1-h)\, w_e, \tag{2.6a}$$

$$\text{where } u_B = -\frac{\partial_f D^2}{2f}, \quad v_B \left(\equiv \frac{\mathrm{d}f}{\mathrm{d}t}\right) = f w_e, \quad C(h) = -\frac{h(1-h)}{f^2}, \quad D^2 = 2f^2 \int_0^x w_e \,\mathrm{d}x \tag{2.6b}$$

For simplicity, in (2.6) we have chosen an exact β-plane such that $f = f_m + \beta_0 y$, where f_m is the mean latitude of a subtropical gyre. (This differs from the standard β-plane in that the $f = f_m + \beta_0 y$ always holds whether f is differentiated or not!)

2.2. *The solution*

The characteristic equations for (2.6*a*) are

$$\frac{\mathrm{d}t}{\mathrm{d}s} = 1, \quad \frac{\mathrm{d}f}{\mathrm{d}s} = v_B = f w_e, \quad \frac{\mathrm{d}h}{\mathrm{d}s} = -(1-h)\, w_e(x, f, t), \tag{2.7a–c}$$

$$\frac{\mathrm{d}x}{\mathrm{d}s} = u_B(x, f, t) - \frac{h(1-h)}{f^2} = -\left(f^2 \int_0^x \frac{w_e \,\mathrm{d}x_f}{f}\right) - \frac{h(1-h)}{f^2}. \tag{2.7d}$$

The initial conditions for characteristics are

$$(t, f, h, x)|_{s=0} = (t_i, f_i, h_i, x_i). \tag{2.8}$$

Division of (2.7*b*) and (2.7*c*) recovers the potential vorticity conservation along the characteristics

$$\frac{\mathrm{d}}{\mathrm{d}s}\left(\frac{f}{1-h}\right) = 0 \quad \text{or} \quad \frac{f}{1-h} = \frac{f_i}{1-h_i}. \tag{2.9}$$

Eastern boundary disturbances are the part of the solution whose characteristics or wave rays start from the eastern boundary. (A complete discussion of the solution in the entire gyre is presented in Liu 1991, 1993*b*). If disturbances are generated along the eastern boundary $x = 0$ by the interface depth $h_e(f, t)$ at time t_i and on latitude f_i, we have the initial conditions

$$x_i = 0, \quad h_i = h_e(f_i, t_i). \tag{2.10}$$

Here we will only consider the waves forced by eastern boundary upwelling $\partial_t h_e \neq 0$ and in the interior the Ekman pumping is assumed steady. Furthermore, the Ekman pumping is chosen to be zonally independent

$$w_e = w_e(f). \tag{2.11}$$

With these assumptions, (2.7*a*, *b*) can be solved immediately as

$$t = t_i + s, \tag{2.12a}$$

$$s = \int_{f_i}^{f} \mathrm{d}\mu/\mu w_e(\mu) \quad \text{or implicitly} \quad f = \hat{f}(f_i, s). \tag{2.12b}$$

Using potential vorticity conservation (2.9) to replace the h-equation (2.7*c*) and noting the initial conditions in (2.10), we have the h-solution

$$h = 1 - [1 - h_e(f_i, t_i)]f/f_i, \tag{2.12c}$$

where f is given in (2.12*b*). Finally, for the x-equation, we use the differential form of (2.12*b*) $\mathrm{d}s = \mathrm{d}f/fw_e(f)$ to replace the characteristic variable s by f in (2.7*d*). Then, noting (2.7), (2.9), (2.10) and (2.12*c*), (2.5*d*) can be integrated along the characteristics (thus f_i, f_i are constants) to give

$$x = [h^2 - h_e^2(f_i, t_i)]/2f^2 w_e(f). \tag{2.12d}$$

The f and h are determined in (2.12*b*, *c*). Equations (2.12*a–d*) give the solution forced by eastern boundary disturbances in the characteristic coordinates. The solution in the (t, x, f)-coordinates can be obtained by cancelling s, t_i, f_i among (2.12). In the special case with $h_e = 0$, (2.12*d*) alone gives the explicit solution $h^2 = 2f^2 w_e(f)\, x$, which is the shadow zone solution (in a two-layer model) of the classic LPS ventilated thermocline (Luyten, Pedlosky & Stommel 1983). The thermocline deepens westward in the subtropical gyre.

3. Planetary wave breaking: no Ekman pumping

The breaking of free waves (i.e. $w_e = 0$) is investigated in this section. The approach developed here will be used in §4 for more complex cases. For simplicity, the eastern boundary interface is chosen to be flat and to vary temporally, i.e.

$$h_e = h_e(t). \tag{3.1}$$

After using this as the initial conditions for characteristics $h_i = h_e(t_i)$, the parametric solution for a free wave is directly derived from (2.7) with $w_e = 0$:

$$x = -\frac{h_e(t_i)[1 - h_e(t_i)]}{f^2}(t - t_i), \tag{3.2a}$$

$$h = h_e(t_i), \tag{3.2b}$$

where $f = f_i$ has been used. Hereafter (unless otherwise specified) the disturbances are

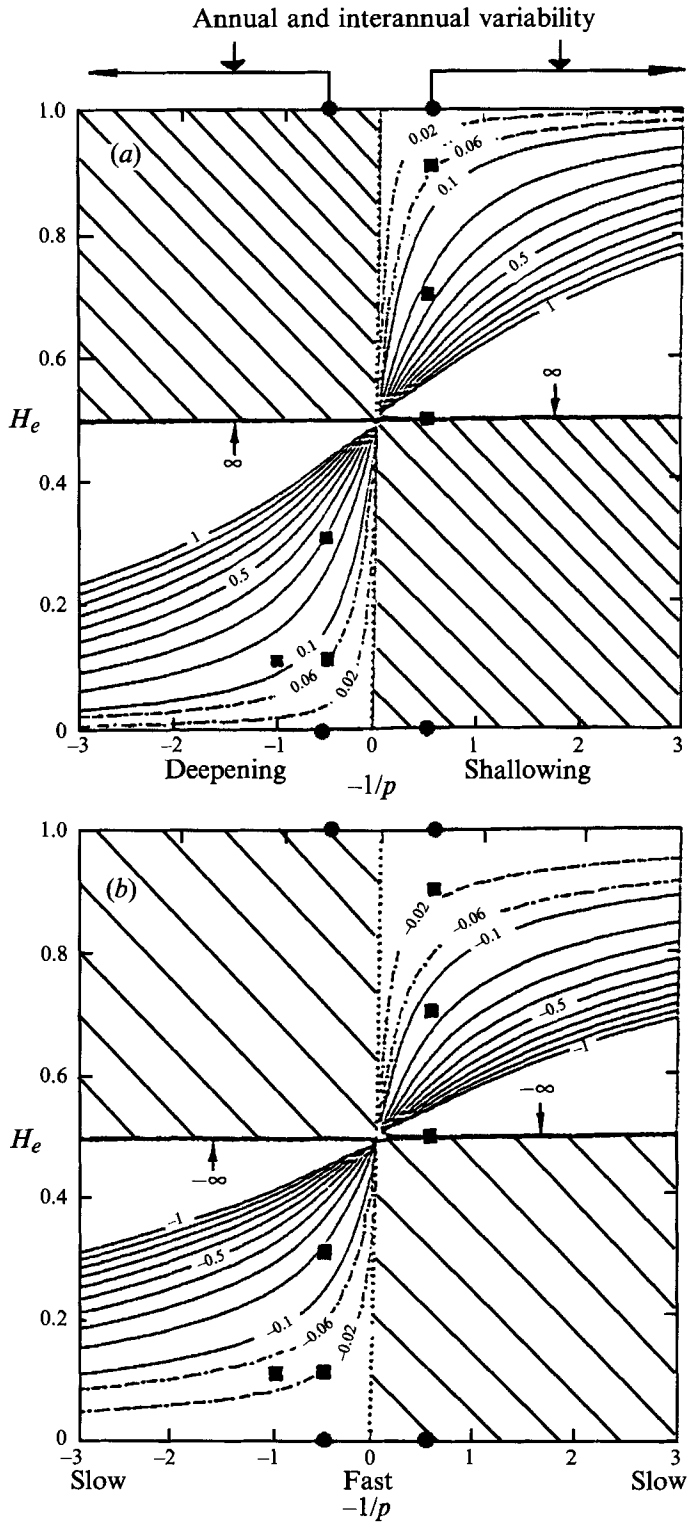

FIGURE 2. The first breaking times and positions for free waves. The horizontal axis is $-1/p$ and the vertical axis is H_e. Hatched regions show the parameters for which no breaking will occur even in an

generated at the eastern boundary such that the interfaces move vertically at a constant speed p, from the initial depth H_e to the final depth H_{e1}, which satisfy $0 \leqslant H_e$, $H_{e1} < 1$, i.e.

$$h_e(t) = \begin{cases} H_e + pt & \text{if} \quad 0 \leqslant t \leqslant T \equiv (H_{e1} - H_e)/p > 0 \\ H_{e1} & \text{if} \quad t > T. \end{cases} \tag{3.3}$$

A downwelling is represented by $p > 0$ and $H_e < H_{e1}$, while an upwelling is represented by $p < 0$ and $H_e > H_{e1}$. The observed maximum speeds of interfaces varying at annual and interannual scales are no more than twice the typical Ekman pumping speed, i.e. $|p| \leqslant 2$. In fact, a typical dimensional Ekman pumping speed is $w_e^* \sim 0.5 \times 10^{-4}$ m s$^{-1} \sim$ 15 m year^{-1}. Observations show that the maximum amplitude of interface variation is below 15 m for annual variation and below 90 m for interannual variation (say with period longer than 6 years) (e.g. Tabara, Thomas & Ramsden 1986). The corresponding dimensional speed is then $p^* \sim 15$ m/0.5 year ~ 90 m/0.5 $\times$ (6 years) $\sim 2w_e^*$. Since the non-dimensional $p = p^*/w_e^*$ (see (2.5) for the scaling of time), annual and interannual variability has the non-dimensional speed range of about $|p| \leqslant 2 \sim O(1)$.

3.1. *The approach*

From the eastern boundary, a perturbation wave is radiated into the interior. This wave may break because of nonlinear steepening $C \sim h(1-h)$. We shall derive the time and position of first breaking. In order to generalize the approach for later cases, the parametric solution (3.2) is put in a general form

$$x = x(t, f, t_i), \quad 0 \leqslant t_i \leqslant T, \tag{3.4a}$$

$$h = h(t, f, t_i). \tag{3.4b}$$

Physically, (3.4) says that at a time t and a latitude f, the disturbance excited along the eastern boundary at a previous time t_i reaches the zonal position $x(t, f, t_i)$. The disturbed interface now is $h(t, f, t_i)$. On a fixed latitude f, a breaking time t_b occurs when the zonal profile is vertical, i.e. $\partial_h x|_{f, t_b} = 0$. In (3.4), this is equivalent to

$$\partial_{t_i} x = 0. \tag{3.5}$$

Breaking times are then obtained from (3.4a) and (3.5) as

$$t_b = t_b(t_i, f) \quad \text{with} \quad t_b \geqslant t_i. \tag{3.6}$$

Hence, along the latitude f, the interface becomes vertical at time t_b on the wave front that leaves the eastern boundary at $t = t_i$. The first breaking time t_0 on the latitude f is the minimum of the family of breaking times in (3.6), i.e.

$$\text{the first breaking time:} \quad t_0 = \min\{t_b\}_{t_i \in [0, T]}. \tag{3.7a}$$

The first breaking position x_0 and depth h_0 are then obtained, by substituting (3.7a) into (3.4a, b), as

$$x_0 = x(t_0, f, t_{i0}), \quad h_0 = h(t_0, f, t_{i0}), \tag{3.7b}$$

where t_{i0} is the t_i at which t_b reaches its minimum as in (3.7a). Mathematically, the above method is equivalent to deriving the envelope of the family of characteristics in (3.4a) as in classical methods.

---

unbounded ocean. The $t_0 > 1$ and $x_0 < -1$ contours are not drawn, where the breaking is unlikely to take place within a basin of a realistic width. (*a*) The first breaking time: the observed maximum annual and interannual forcing speeds are marked on the top, and the black squares mark the parameters used later in figure 3. (*b*) The first breaking position at $f = 0.6$ (about 30°).

3.2. *Free wave breaking*

Substituting the free wave solution (3.2) and the eastern boundary perturbation (3.3) into (3.5) yields the breaking time

$$t_b = t_i + \frac{h_e(t_i)[1-h_e(t_i)]}{p[1-2h_e(t_i)]} \quad \text{for} \quad 0 \leqslant t_i \leqslant T. \tag{3.8}$$

Differentiating (3.8) gives

$$\partial_{t_i} t_b = 2[1 + h_e(1-h_e)/(1-2h_e)^2] > 0. \tag{3.9}$$

This means that a disturbance which is excited later will break later. Hence the first breaking time occurs at the earliest disturbance wave front with $t_i = 0$. With the aid of (3.3) and (3.8), the first breaking time takes the form

$$t_0 = t_b|_{t_i=0} = \frac{H_e(1-H_e)}{p(1-2H_e)}. \tag{3.10}$$

The corresponding breaking distance x_0 is obtained by substituting (3.10) into (3.2*a*), and by using $t_i = 0$ in (3.3),

$$x_0 = -\frac{H_e(1-H_e)}{f^2} t_0. \tag{3.11}$$

It is interesting to see that the first breaking time and position are independent of the disturbance amplitude $H_{e1} - H_e$ (there is no H_{e1} dependence in (3.10) and (3.11)). Hence, the occurrence of breaking is determined only by the speed and depth of the perturbation along the eastern boundary. For eastern boundary conditions more general than (3.3), calculations for some other examples also show that the first breaking time and position are mainly determined by the interface depth and maximum vertical speed of the perturbation.

To study the breaking in more detail, we plot the t_0 and x_0 in the speed, depth parameter plane in figure 2. Figure 2(*a*) displays t_0, which is independent of f as seen in (3.10), as a function of $-1/p$ and H_e. The speed ranges for the observed annual and interannual variation ($|p| \leqslant 2$) are also marked on the top. A shallowing has $-1/p > 0$ on the right half-plane and a deepening has $-1/p < 0$ on the left half. The non-breaking parameter region is hatched. It is seen from figure 2(*a*) that at the fast speed, $|p| = 2$, breaking events occur within about one advective time $t_0 \leqslant O(1)$ for interfaces at most depths. Figure 2(*b*) illustrates the corresponding x_0 at latitude $f = 0.6$. It indicates that most of the breaking occurs within the basin $|x_0| \leqslant O(1)$. For a slower speed p, the H_e range for breaking gets smaller and breaking tends to be trapped on interfaces near the surface and bottom. If the speed is very slow, i.e. $p \to 0$, we have $x_0 \to -\infty$. Thus, breaking will not take place within a finite basin although in principle it may occur in an ocean unbounded to the west.

As we have seen in figure 2, breaking occurs rapidly for an interface near the surface or bottom, but breaking occurs very late for an interface near mid-depth. This can be explained as follows. Under a perturbation δh, the local Rossby wave speed is expanded around the mean local depth h_0 as

$$C(h) = C(h_0) + \partial_{h_0} C(h_0)\, \delta h.$$

The first term is the local linear Rossby wave speed while the second term represents

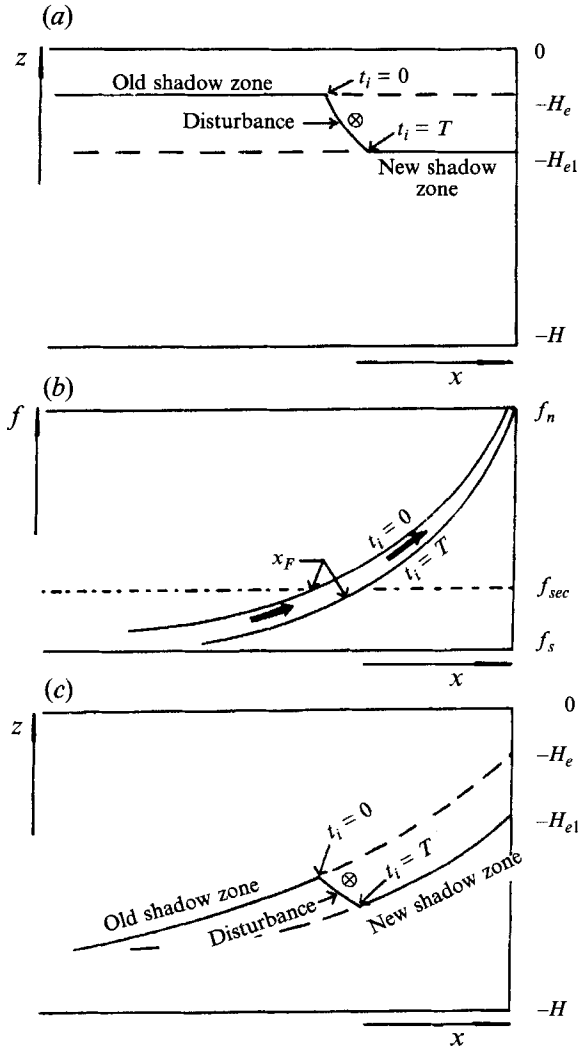

FIGURE 3. A schematic figure of a zonal profile for a downwelling eastern boundary displacement and its associated wave fronts. The solid lines are the zonal profile and the dashed lines represent the continuation of the two shadow zone profiles. (*a*) Free wave zonal profile at $f = f_{sec}$, $W_e = 0$, (*b*) the two-dimensional structure of the breaking front confined by the initial and last wave fronts. The black arrows indicate the thermal wind jet, i.e. $v_T = v_1 - v_2$. (*c*) Zonal profile with Ekman pumping at $f = f_{sec}$, $W_e < 0$. The maximum amplitudes of the breaking fronts are also shown schematically.

the effect of nonlinear steepening. Thus, the intensity of the nonlinear steepening can be measured by

$$\Delta = \frac{\partial_{h_0} C(h_0)\,\delta h}{C(h_0)} = \frac{(1-2h_0)\,\delta h}{h_0(1-h_0)}.$$

For an interface near the surface ($h_0 \to 0$) or bottom (h_0 1), $\Delta \to \infty$, implying a strong nonlinear steepening. On the other hand, for an interface near the middle depth ($h_0 \to 0.5$), $\Delta \to 0$, suggesting a very weak nonlinear steepening.

In addition, to compare with later cases with Ekman pumping, several features are noteworthy in figure 2. First, for breaking to occur, the result of a shallowing, ($p < 0$) at the eastern boundary interface depth H_e is equivalent to a corresponding

deepening ($-p > 0$) at the depth $1 - H_e$ (as reflected about the mid-depth $H_e = 0.5$). In particular, a downwelling causes breaking only when $H_e < 0.5$ while an upwelling causes breaking only for $H_e > 0.5$. Second, both t_0 and x_0 vary monotonically with either H_e or p. Thus, for a faster speed p, or an interface closer to the surface (when $p < 0$) or the bottom (when $p > 0$) of the model ocean, the breaking occurs earlier and closer to the eastern boundary. For the special case $H_e = 0$ (when $p < 0$) or $H_e = 1$ (when $p > 0$), breaking occurs immediately at the eastern boundary, while for $H_e = 0.5$ no breaking will occur at all.

Lastly, it is helpful to introduce a way of judging, directly from figure 2(*a*), if the first breaking time is at the initial front $t_i = 0$. Take the downwelling breaking as an example. In figure 2(*a*), at a fixed downwelling speed $p > 0$, t_0 increases with H_e. This implies that t_0 must occur on the initial $t_i = 0$ front. The reasoning is as follows. Examining the breaking times in (3.8), one sees that the first term on the right-hand side (i.e. t_i) increases with t_i. The second term $h_e(t_i)[1-h_e(t_i)]/p[1-2h_e(t_i)]$ has the same form as the t_0 in (3.10) except that H_e is replaced by h_e. Hence, an increase of t_0 with H_e in figure 2(*a*) means an increase of the second term with (h_e and then) t_i (note $\partial_{t_i} h_e = p > 0$). As a result, t_b in (3.8) increases with t_i, which is consistent with the earlier analytical calculation (3.9), $\partial_{t_i} t_b > 0$. Accordingly, the first breaking time is on the earliest wave front $t_i = 0$. It should be pointed out that for a general eastern boundary perturbation $h_e(t)$, the breaking time may not be the earliest disturbance time (Liu 1991, p. 175).

3.3. *Structures and amplitudes of breaking fronts*

We start by examining the evolution of zonal profiles. A schematic figure of a zonal profile due to a deepening $p > 0$ at a time t is shown in figure 3(*a*). There are three regimes in a typical zonal profile. The western part is the old (before-perturbation) shadow zone (in the absence of Ekman pumping, the whole gyre is filled with a shadow zone in which the thermocline is flat!) which has not been affected by an eastern boundary disturbance. Behind the old shadow zone is the disturbed regime forced by lowering the interface along the eastern boundary. Before the perturbation stops ($t < T$), only these two parts exist. After the perturbation stops ($t > T$), there will be a third part that is the new (after perturbation) shadow zone established near the eastern boundary. The initial ($t_i = 0$) and final ($t_i = T$) disturbance wave fronts are also marked on figure 3(*a*). Before breaking, an earlier wave front is always west of a later wave front. At the first breaking time, a later wave front catches up with an earlier one. The interface becomes vertical at the first breaking position x_0 (this case is not shown in figure 3*a*). Figure 4 plots some examples of the evolution of zonal profiles at $f = 0.6$ (about 30°) calculated from (3.2*a*, *b*) and (3.3). In all figures, the eastern boundary interface varies with an amplitude $\delta h_e = 0.2$ (about 120 m).†

Figure 4(*a–e*) illustrates the evolution for the fastest possible annual and interannual speed $|p| = 2$ (twice the speed of the realistic Ekman pumping speed). The values of t_0 and x_0 are found from figure 2(*a*, *b*) (black squares). The solid lines are the $t = 1$ zonal profiles while the dashed lines indicate the disturbance profiles at earlier times. Figure 4(*a*) depicts a downwelling case with a very shallow interface $H_e = 0.1$. One sees that a strong overturning has appeared on the first disturbance profile at $t = 0.2$. In fact, the wave has already broken long before $t = 0.2$, at $t = 0.06$. After the first breaking time, the solution in (3.2) is no longer valid because of the gravitational instability. Smaller-

† This is too large for observations. It is chosen only for clarity of the figures. In any case, for (3.3), this large amplitude does not change the first breaking times and positions because (3.10) indicates that t_0 (and x_0) depends only on the initial depth H_e but independent of H_{e1}.

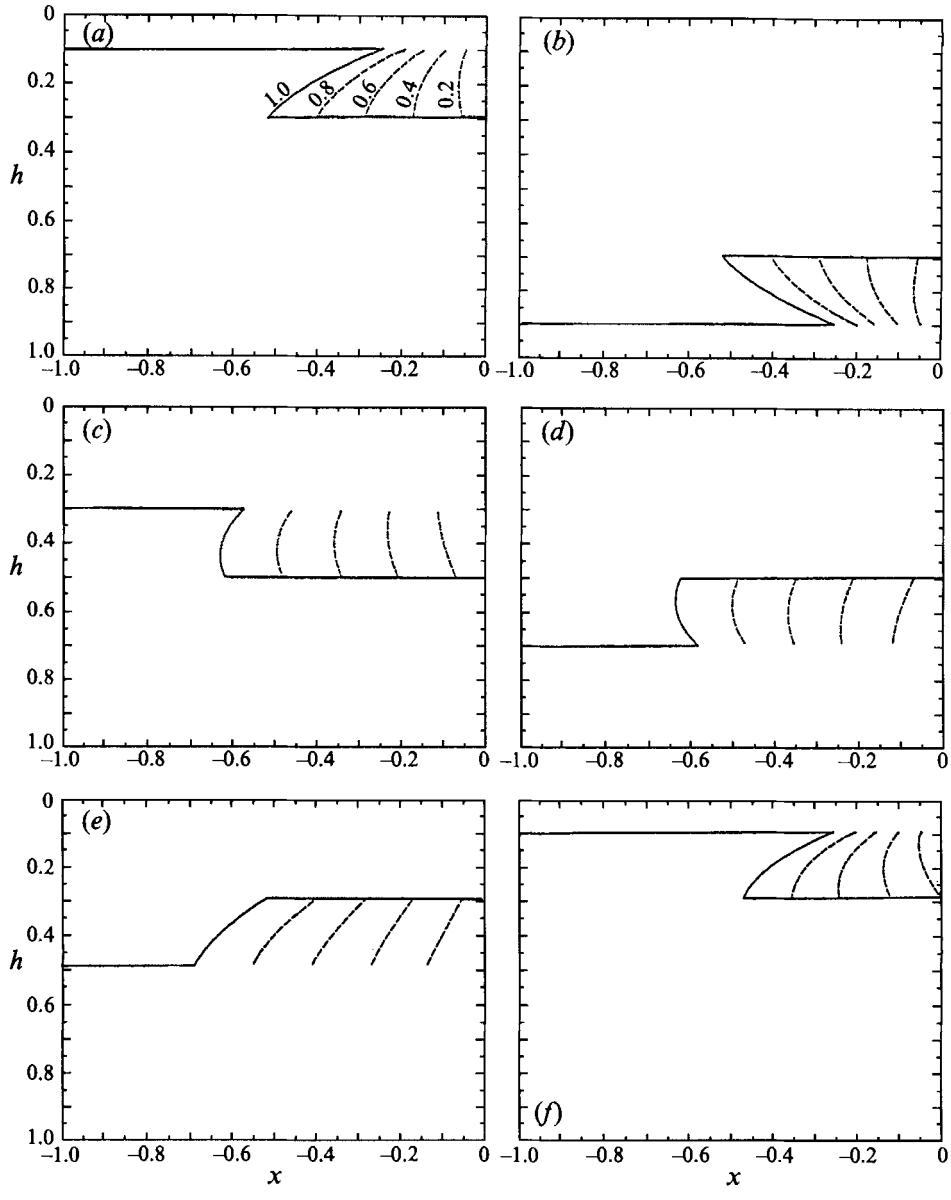

FIGURE 4. Zonal profile evolution for free waves. The eastern boundary interface moves at a constant speed p and the amplitude $|H_{e1}-H_e| = 0.2$. (*a*) $p = 2$, $H_e = 0.1$. (*b*) $p = -2$, $H_e = 0.9$. (*c*) $p = 2$, $H_e = 0.3$. (*d*) $p = -2$, $H_e = 0.7$. (*e*) $p = -2$, $H_e = 0.5$. (*f*) $p = 1$, $H_e = 0.1$. The profiles are all at $t = 0.2$, 0.4, 0.6, 0.8 and 1. The latitude is at $f = 0.6$ (about 30°). (*a*, *b*) $t_0 = 0.06$, $x_0 = -0.02$; (*c*, *d*) $t_0 = 0.3$, $x_0 = -0.18$; (*e*) no breaking; (*f*) $t_0 = 0.13$, $x_0 = -0.04$.

scale process such as friction or relative vorticity will enter. (The fast breaking for shallow interfaces near the eastern boundary has been pointed out by Anderson & Killworth 1979.) Figure 4(*b*) shows the upwelling counterpart of figure 4(*a*). The profile is a mirror imagine of figure 4(*a*) with respect to $H = 0.5$. The t_0 and x_0 are the same as in figure 4(*a*).

If the downwelling disturbance in figure 4(*a*) starts at a greater depth $H_e = 0.3$, figure 4(*c*) indicates that the overturning has not yet appeared on the $t = 0.2$ profile.

In fact, both t_0 and x_0 are delayed by a factor of more than five. Relative to the shallower case, figure 4(*a*), the breaking now takes place far away from the eastern boundary. Figure 4(*d*) is the upwelling breaking counterpart to figure 4(*c*) which has the same t_0 and x_0. Figure 4(*e*) illustrates a shallowing perturbation forced by the same speed as that in figure 4(*b*, *d*) but for $H_e = 0.5$. One sees that breaking will not occur. The last example is figure 4(*f*) where the deepening speed in figure 4(*a*) is reduced by a half to $p = 1$. Equation (3.8) shows that the first breaking time will be twice that in figure 4(*a*).

The reason for downwelling breaking on $H < 0.5$ and upwelling on $H > 0.5$ is simple. Descending h_e causes the disturbance profile to shallow westward. If $h < 0.5$, the local Rossby wave speed $C(h)$ is slower on the western side because $C(h) \sim h(1-h)$ reaches its maximum at $h = 0.5$. Therefore, a later disturbance on the eastern side will travel faster to catch up with a previous disturbance, causing a downwelling breaking. The opposite occurs for ascending h_e.

The flow field for a downwelling breaking front is the opposite to that for an upwelling breaking front. A downwelling breaking must produce a northward thermal wind jet along the breaking front, as drawn schematically in figure 3(*a*), while an upwelling breaking produces a southward thermal wind jet.

The two-dimensional structure of the breaking front is simply the linear β-dispersion shape $x \sim 1/f^2$. This is because the first breaking time (3.10) is independent of latitude, so the only f-dependency for the breaking position (3.11) is the $1/f^2$ factor. A schematic figure of the two-dimensional (before breaking) disturbance structure (bounded by the initial and final disturbance fronts at $t_i = 0$ and T) is drawn in figure 3(*b*). Later, when the breaking occurs, the breaking front will be sandwiched by the initial and final disturbance fronts.

Although the amplitude of the breaking front is beyond the scope of our model, some preliminary results can still be obtained. We see that the disturbance is vertically bounded by the interfaces of the old and the new shadow zones:

$$h_{\text{old shadow zone}} = H_e, \quad h_{\text{new shadow zone}} = H_{e1}. \tag{3.12}$$

Therefore, we can estimate the upper bound on the intensity of the breaking front as

$$\text{Front intensity} \sim |h_{\text{old shadow zone}} - h_{\text{new shadow zone}}| = |H_{e1} - H_e|. \tag{3.13}$$

This shows that the intensity of a breaking front is determined by the amplitude of the perturbation (although we have seen in (3.10) and (3.11) that the occurrence time and position of breaking are independent of the amplitude).† Furthermore, in the absence of an Ekman pumping, (3.11) states that the shadow zone thermocline is flat. Thus, (3.13) suggests that the intensity of the breaking front is the same everywhere on the front.

4. Planetary wave breaking: with Ekman pumping

In the presence of Ekman pumping, there will be both a two-dimensional barotropic flow and an external forcing. No general approach or conclusions about the wave breaking in the presence of a two-dimensional flow are available. Nevertheless, the analytical solutions in (2.12) make it possible to examine the breaking condition.

† As one reviewer pointed out, eventually, when relative vorticity becomes important, it is conceivable that up to a certain amplitude, the size of the front may also be independent of the forcing amplitude. As in many nonlinear waves, there may be a limit which is intrinsic to the system and independent of the forcing.

4.1. *Forced wave breaking*

To understand the basic effect of Ekman pumping on breaking, we adopt the simplest Ekman pumping – a spatially uniform one:

$$w_e(f) = W_e. \tag{4.1a}$$

Then, the f-solution in (2.12b) can be solved as $f = f_i\, e^{W_e s} = \hat{f}$. This can be reversed to represent the initial latitude as

$$\hat{f}_i(f, s) = f e^{-W_e s}. \tag{4.1b}$$

After substituting (4.1a, b) into (2.12), the solutions with t_i as a parameter are obtained as

$$x = \frac{\{1-[1-h_e(t_i)]\, e^{W_e(t-t_i)}\}^2 - h_e(t_i)^2}{2f^2 W_e} = x(t, f, t_i), \tag{4.2c}$$

$$h = 1-[1-h_e(t_i)]\, e^{W_e(t-t_i)} = h(t, f, t_i). \tag{4.2d}$$

Similar to the free wave case, taking the eastern boundary perturbation (3.3), the breaking time is determined, by setting $\partial_{t_i} x = 0$, as

$$t_b = t_i + \frac{1}{W_e} \ln [J(h_e, W_e/p)], \tag{4.3a}$$

or

$$p(t_b - t_i) = \frac{1}{W_e/p} \ln [J(h_e, W_e/p)], \tag{4.3b}$$

where

$$(1-h_e) J^2 - J + \frac{h_e}{1+(1-h_e)\, W_e/p} = 0. \tag{4.3c}$$

A physically realistic breaking occurs after the disturbance is generated or $t_b - t_i \geqslant 0$. Thus, we require that $0 \leqslant J \leqslant 1$. J is readily solved from (4.3c) as

$$J\pm = \frac{1}{2(1-h_e)} \left\{ 1 \pm \left[1 - \frac{4h_e(1-h_e)}{1+(1-h_e)\, W_e/p} \right]^{\frac{1}{2}} \right\}. \tag{4.3d}$$

The sign is chosen such that t_b gives the minimum and positive $t_b - t_i$ if available. The free wave limit (3.8) can be recovered from (4.3b) in the limit $W_e/p \to 0$.

It will be shown soon that the first breaking time occurs at the initial wave front $t_i = 0$. Therefore, from (4.3b) and (3.3) the first breaking time satisfies

$$pt_0 = \frac{1}{W_e/p} \ln [J(H_e, W_e/p)]. \tag{4.4}$$

The corresponding position is obtained by substituting (4.4) into (4.2a) to give

$$x_0 = \frac{\{[1-(1-H_e)\, e^{W_e t_0}] - H_e^2\}}{2f^2 W_e}. \tag{4.5}$$

As in the free wave case of (3.10) and (3.11), the first breaking time and position are independent of the amplitude of the perturbation $H_{e1} - H_e$. Thus, the occurrence of breaking is determined only by the vertical speed of the perturbtion and the interface depth at which the disturbance occurs.

With $w_e = -1$, t_0 and x_0 are plotted in figure 5, which is arranged similarly to figure

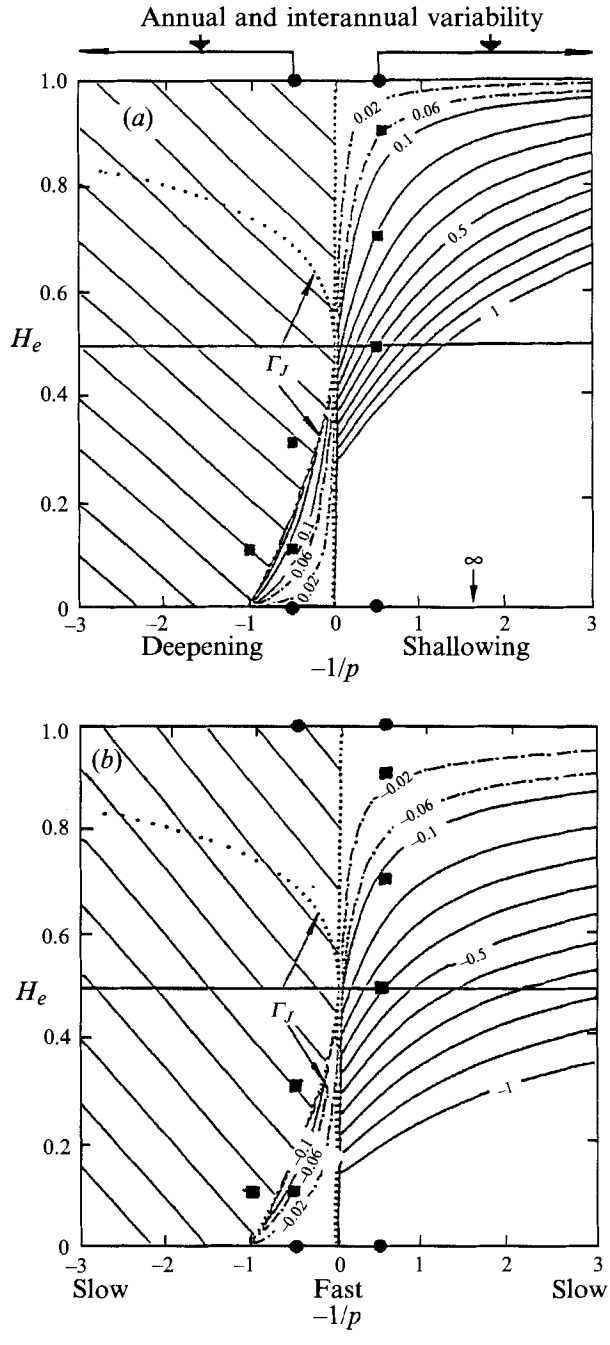

FIGURE 5. The first breaking times and positions with uniform Ekman pumping $w_e(f) = W_e = -1$. The parameters in each figure correspond those in figure 2. (*a*) t_0. (*b*) x_0 at $f = 0.6$ (about 30°). In comparison with the free wave case in figure 2, the downwelling breaking domain is severely reduced while the upwelling breaking domain is greatly enhanced (see the text for a fuller discussion).

2. t_0 is independent of f and is displayed in figure 5(*a*). One sees that t_0 increases monotonically with H_e for deepening and decreases monotonically with H_e for shallowing. Using an argument similar to that for free waves (at the end of §3.2), we know that the first breaking time must occur on the initial wave front $t_i = 0$.

The most striking difference between figure 5(*a*) and the free wave case of figure 2(*a*) is that t_0 is not at all symmetrical with respect to the centrepoint $(-1/p, H_e) = (0, 0.5)$, particularly for a perturbation speed comparable with or slower than the Ekman pumping speed ($p \leqslant O(1)$), which is just the speed of interest for annual and interannual variations. In comparison with the free wave in figure 2(*a*), the upwelling breaking time is shortened and its parameter domain is substantially enlarged. On the contrary, the downwelling breaking time is delayed and its domain is severely reduced. Hence, imposing Ekman pumping will enhance upwelling breaking but suppress downwelling breaking.

In more detail, the upwelling breaking now occurs for interfaces from the top to the bottom of the model ocean. At a fixed ascending speed p, the first breaking time increases monotonically from 0 to ∞, as H_e varies from 0 to 1 (as opposed to varying from 0 to 0.5 as in the free wave case.) In particular, near or slightly above mid-depth $H_e \lesssim 0.5$, if a shallowing is faster than or comparable with the Ekman pumping ($p \leqslant O(1)$), an upwelling breaking occurs within an advective time ($t_0 < O(1)$). This is in sharp contrast to the free wave case where no upwelling breaking occurs at all if $H_e \leqslant 0.5$ (see figure 2*a* near $H_e = 0.5$ for shallowing). The implication is that for interfaces near and above the mid-depth, an upwelling breaking is qualitatively changed from non-breaking to breaking.

In contrast to the upwelling case, for a downwelling breaking, fast downwelling ($p \gg 1$) is similar to the free wave case. However, a qualitative difference from the free wave appears for descending speed comparable or slower than the Ekman pumping. In the parametric plane, there is a (internal) marginal curve given by the dotted line (Γ_J see figure 5) on the edge of downwelling breaking domain. This curve is $W_e/p = -(1-2H_e)^2/(1-H_e)$, which is derived by substituting $t_i = 0$ and (3.3) into (4.3*d*) and then setting the square root in (4.3*d*) to zero. As far as the J-value is concerned, Γ_J divides the complex conjugates of J on the left from the real J on the right. On Γ_J, the breaking time is finite. In fact, at each depth, Γ_J gives a cutoff (or slowest descending) speed

$$p_c(H_e) = -W_e(1-H_e)/(1-2H_e)^2 > 0. \tag{4.6}$$

For a descending speed slower than p_c, downwelling breaking will not occur. The minimum speed p_c in (4.6) is

$$\min\{p_c\} = -w_e,$$

implying no downwelling breaking at any depth if the downwelling speed is slower than the surface Ekman pumping ($p < -w_e$). As H_e deepens from 0 to 0.5, Γ_J varies from $W_e/p = -1$ to $W_e/p = 0$ and the associated cutoff speed (4.6) increases from $-w_e$ to ∞. Thus, away from the surface the cutoff speed increases and breaking becomes less likely to take place.

Physically, it is hard to understand exactly how and why the breaking conditions are altered, partly because the effect of the mean flow is coupled with that of the external Ekman pumping. Nevertheless, a rudimentary explanation is offered here. Relative to a water particle forced downward (by the surface Ekman pumping) with a speed $w < 0$, an upwelling h_e at an ascending speed $p < 0$ has a stronger ascending speed $p + w < p < 0$. In other words, relative to the water particle, the upwelling speed is

enhanced, which in turn results in a stronger upwelling breaking tendency and an earlier breaking time. However, with respect to this downward particle, a descending h_e at the speed $p > 0$ has a relatively weaker descending speed $p+w < p > 0$. In particular, when the descending is slower than the downward speed of the particle $0 < p+w < p$, h_e moves upward relative to that particle. As a result, downwelling breaking will not occur. This offers an explanation for why downwelling breaking abruptly disappears when $p < -w_e$.

In a basin with a finite zonal extent, breaking occurs only when the x_0 is within the basin. The x_0 derived from (4.5) is plotted in figure 5(*b*) at latitudes $f = 0.6$ (about 30°). Similarly, to t_0, here x_0 differs substantially from the free wave case. In the figure, the x_0 are much closer to the eastern boundary than the free wave case in figure 4(*b*).

In summary, under a mean downward Ekman pumping as in a subtropical gyre, downwelling breaking is severely suppressed and the breaking time is delayed. For descending speeds slower than the Ekman pumping, there will be no downwelling breaking. In addition, downwelling breaking tends to be trapped on interfaces near the surface. In contrast, upwelling breaking is greatly enhanced by the mean downward Ekman pumping and the breaking times are shortened. Shallowing breaking even appears on interfaces within the upper half of the ocean.

4.2. *Structures and amplitudes of breaking fronts*

In the presence of Ekman pumping, (2.12*d*) alone gives explicitly the shadow zone solution (if $h_e = H_e = \text{constant}$)

$$h = (2f^2 w_e(f)\, x + H_e^2)^{\frac{1}{2}}. \tag{4.7}$$

Now, the interface deepens westward. Schematically, a zonal profile after an eastern boundary disturbance is as in figure 3(*c*). This differs from the free wave case in figure 3(*a*) in that now the disturbance is advected downward as it advances westward.

Figure 6 shows some examples of the evolution of zonal profiles at $f = 0.6$. The parameters in figure 6(*a–f*) correspond to those in figure 4(*a–f*) respectively except now with Ekman pumping $w_e = -1$. For the strong annual and interannual deepening on a shallow interface with $H_e = 0.1$, comparing figure 6(*a*) with the free waye case in figure 4(*a*), one sees that the first breaking time and position are delayed by a factor of about three. Yet the corresponding upwelling breaking in figure 6(*b*) has t_0 and x_0 only slightly earlier than the free wave case in figure 4(*b*). A dramatic change occurs if the interface is deeper, say $H_e = 0.3$ as in figure 6(*c*), or the deepening speed is reduced, say by a half, as in figure 6(*f*); now downwelling breaking does not occur even in an unbounded ocean while the free wave in figures 4(*c*) or 4(*f*) breaks early in the eastern part of the basin. These two cases are located in the parameter plane in the non-breaking domain (the hatched region in figure 5*a*, *c*). The upwelling case corresponding to figure 6(*c*) is shown in figure 6(*d*). The first breaking time and position are shortened by about 40% compared to the free wave in figure 4(*d*). If the interface starts further up within the upper half of the ocean, a significant change appears for the upwelling breaking. Although the free wave in figure 4(*e*) will not break, upwelling breaking will take place in the presence of Ekman pumping as shown in figure 6(*e*). Combining figure 6(*e*) with figure 6(*c*), one can imagine an interesting phenomenon. Under a periodic h_e forcing, the disturbance will create an upwelling breaking front on an interface in the upper half of the ocean where otherwise a downwelling breaking front will be expected in the absence of Ekman pumping.

Another difference from the free wave case is that all the disturbances now slide down the steady shadow zone thermocline because of the downward Ekman pumping

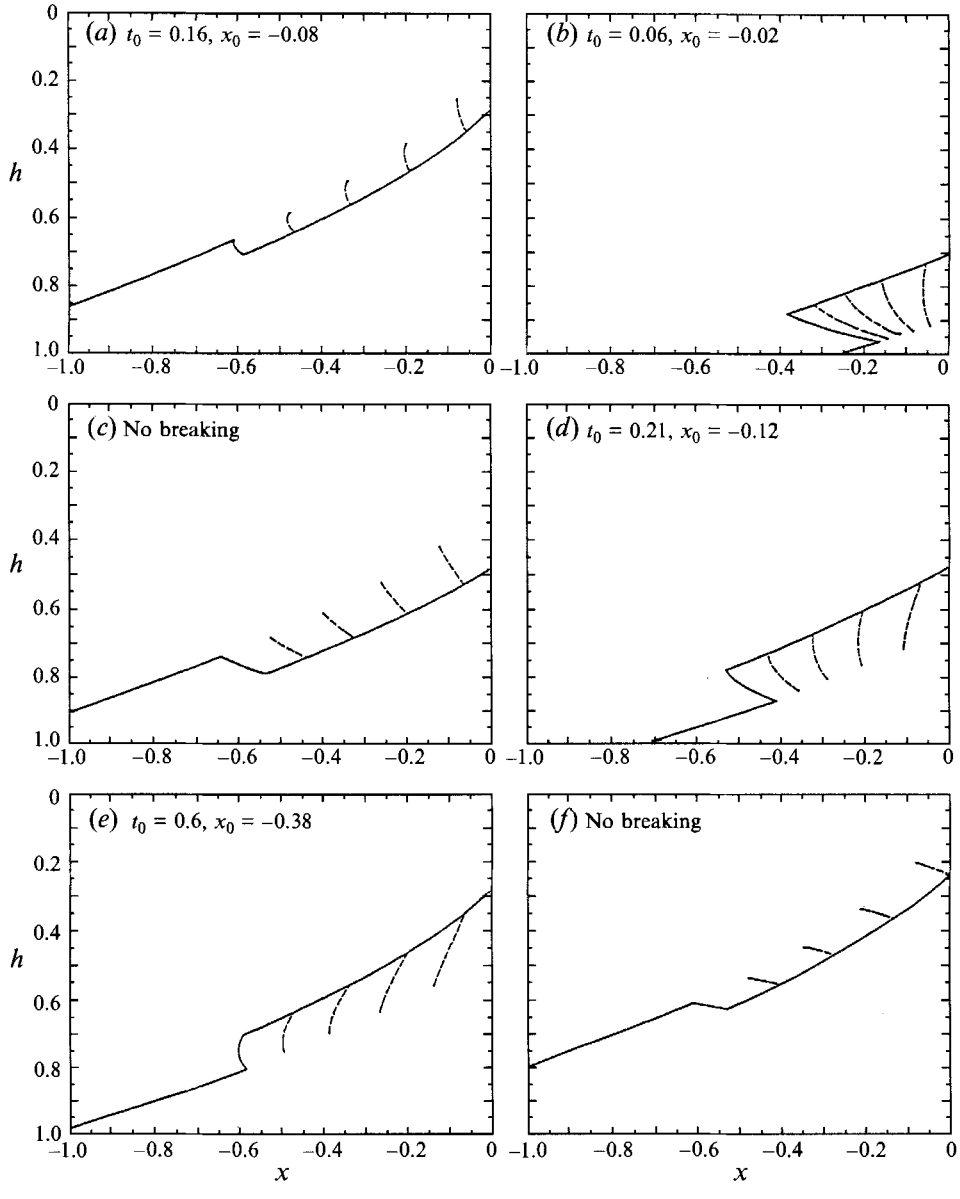

FIGURE 6. Zonal profile evolution for waves in the presence of uniform Ekman pumping $w_e = -1$. The eastern boundary condition is the same as in figure 4. Parameters in (*a–f*) correspond to those in figure 4(*a–f*).

(figure 6). This vertical propagation provides another explanation for the suppressed downwelling breaking and enhanced upwelling breaking. Initially, a deepening disturbance starting at $h \sim H_e < 0.5$ will of course create a downwelling breaking tendency (i.e. a westward shoaling interface) that can only break for $h < 0.5$. Its profile is becoming steeper due to the nonlinear steepening. However, the disturbance also propagates downward. The perturbation may penetrate to the deeper half of the ocean ($h > 0.5$) before breaking. After it descends to the lower half of the ocean, the perturbation with the downwelling breaking tendency (shoaling towards the west) will never break. A similar argument applies to a disturbance forced by a shallowing.

The structure of the breaking front can also be estimated according to (3.12). Now, the old and the new shadow zones are (see (4.7))

$$h_{\text{old shadow zone}} = (2f^2 w_e(f)\, x + H_e^2)^{\frac{1}{2}}, \quad h_{\text{new shadow zone}} = (2f^2 w_e(f)\, x + H_{e1}^2)^{\frac{1}{2}}.$$

As a result, we have the upper bound for the amplitude of a breaking front occurring at $x = x_0, f = f_0$ as

$$\Delta h \leqslant |h_{\text{old shadow zone}} - h_{\text{new shadow zone}}| = \frac{|H_{e1}^2 - H_e^2|}{(2f_0^2 w_e(f_0)\, x_0 + H_e^2)^{\frac{1}{2}} + (2f_0^2 w_e(f_0)\, x_0 + H_{e1}^2)^{\frac{1}{2}}}. \tag{4.8}$$

It is seen that this upper bound is determined by two factors: the amplitude of the initial displacement $H_{e1} - H_e$ and the distance from the eastern boundary x_0. The upper bound increases with the initial amplitude and decreases westward monotonically. The zonal decay is related to the strength of the Ekman pumping ($w_e(f)$). The stronger the Ekman pumping is, the faster the decay will be. In the absence of Ekman pumping, there is no zonal decay, as has been seen in the free wave case (figure 4)†. The upper bound in (4.8) only gives a local upper bound and prohibits any direct estimate of the amplitude of a breaking front. Nevertheless, it still seems reasonable to speculate that the amplitude of breaking fronts will increase with initial amplitude and decrease away from the eastern boundary. This leads to two important deductions. First, breaking fronts occurring far from the eastern boundary are usually weak. Secondly, although both an interannual variation and an annual variation with the same maximum speed have comparable first breaking times and positions (see the discussion following (4.5)), the interannual variation will create a stronger breaking front than the annual variation because of the longer time, and therefore a larger amplitude of the interannual variation. In other words, the occurrence of the breaking (the breaking time and position) is mainly determined by the maximum vertical speed of the disturbance, while the intensity of the breaking front mainly depends on the amplitude of the disturbance.

Finally, we show that in the presence of mean flow, the breaking positions are changed qualitatively. Re-examining the free wave in figure 2 or (3.2), one sees that an infinite breaking time must occur at a position infinitely west of the eastern boundary (and thus out of the basin). Therefore, the only free waves that break, are those with $t_0 \leqslant O(1)$ (so that $x_0 \leqslant O(1)$). But now in figure 5 or (4.5), breaking positions are finite even for breaking times approaching infinity (on the shallowing half-plane near $H_e \to 0$ in figure 5*a*, *b*).

These finite breaking positions are caused by the two-dimensional barotropic flow field, which tends to carry wave energy southward while they propagate westward. In fact, in the thermocline it is this mean flow field that causes the different zones (pool zone, ventilated zone and shadow zone). Waves forced along the eastern boundary can only propagate in the shadow zone which is bounded to the west by the shadow zone boundary (which is then connected to a ventilated zone or pool zone). Therefore, no matter how long it takes, breaking will occur within the shadow zone boundary. Moreover, since in (4.4) t_0 is independent of f, (4.5) says that a breaking position exhibits a linear β-dispersion shape as is the case for the free wave. Therefore, breaking fronts occur closer to the eastern boundary in the north than in the south. Noting the

† This upper bound actually applies to non-breaking waves too. Therefore, a disturbance tends to decrease in its amplitude as it propagates westward and downward. This has been explained in Liu (1993*c*). The physical mechanism for this decay is a divergent group velocity field.

westward decay of breaking front intensity discussed in (4.8), we come to another important conclusion: breaking fronts, if any, are usually stronger towards the north.

5. Summary and discussion

In this analysis it is found that planetary wave breaking is affected significantly by Ekman pumping and its associated mean flow. In the presence of Ekman pumping, breaking in a downwelling disturbance is suppressed and the breaking time is delayed; breaking in an upwelling disturbance is enhanced and its time is shortened. The breaking of annual and interannual disturbances will be significantly altered. In particularly, downwelling breaking will not occur except for interfaces near the surface.

The breaking times and positions are mainly determined by the maximum vertical perturbation speed while the intensity of the breaking front mainly depends on the amplitude of the perturbation. The intensity of a breaking front increases with the amplitude of the forcing, but decreases with the distance from the eastern boundary. The positions of breaking fronts are significantly closer to the eastern boundary with two-dimensional mean flow in the northern part. On the other hand, the orientation of a breaking front in the northeast–southwest direction. (This is not valid near the southern boundary of a subtropic gyre because a uniform Ekman pumping is used in §4. See Liu 1993*a*). Thus, the intensity of a breaking front tends to be stronger towards the north.

In the presence of spatially varying Ekman pumping, we can similarly study the breaking of disturbances generated at the eastern boundary. A detailed discussion is presented in Liu (1991), where Ekman pumping with both linear and parabolic profiles in latitude are discussed. It is found that the breaking in the northern subtropical gyre is similar to the free wave breaking case in §3. In contrast, breaking in the southern subtropical gyre is similar to the uniform Ekman pumping case studied above. Physically, this difference occurs because of the southward mean flow. In our model, the southward mean flow carries the effect of the Ekman pumping southward. In the northern subtropical gyre there is very little wave energy coming from the north, which in turn results in a breaking similar to a free wave case. But in the southern part much wave energy arrives from the north and middle of the basin and therefore the influence of Ekman pumping is stronger. In addition, within each half-basin, near the middle of the basin, the breaking is more similar to a uniform Ekman pumping case compared with the breaking occurring near the gyre boundaries. The physics is simple. Near the middle of the gyre, the magnitude of the local Ekman pumping is stronger.

One should be cautious in applying the theory here to a continuously stratified thermocline. This is because we are not sure if an interface in a two-layer model at certain depth corresponds to an isopycnal in a continuously stratified thermocline at the same depth. Nevertheless, it is still interesting to compare the results here with observations. The Subtropical Front is trapped near the surface and is accompanied by a northward baroclinic jet. The front found during the POLYMODE Local Dynamics Experiment (McWilliams *et al.* 1983; Hua *et al.* 1986) in the North Atlantic extends very deep and is accompanied by a southward baroclinic jet. These are consistent with our theory here. A downwelling breaking front, which is accompanied by a northward thermal wind jet, is trapped near the surface. An upwelling breaking front, which is accompanied by a southward thermal wind jet, can extend very deep. All observed fronts have slopes consistent with a northeast–southwest orientation.

Finally, note that without a statistically steady eastern boundary (or localized wind or diabatic) forcing, it is unlikely that the temporal breaking phenomena discussed here

are mainly responsible for the observed statistically stationary fronts such as the Subtropical Front. However, it is possible that some temporal behaviour and finer structures observed within these mean fronts (Niiler & Reynolds 1984) are produced by the breaking of (more general) planetary waves which are caused not only by the eastern boundary upwelling or downwelling but also by local wind or buoyancy flux. The breaking can be caused mainly by the nonlinear steepening of a Rossby wave, which propagates along a smooth thermocline, as discussed here.

It is also possible for breaking to be produced by a second mechanism not investigated in this paper. That is the effect on nonlinear Rossby waves of the thermocline structure associated with a mean frontal structure (which is formed by some other mechanisms). In this case, breaking occurs because the rapid spatial variation of the basic thermocline may produce a strong variation of local Rossby wave speed within the mean front, which in turn causes breaking of the nonlinear Rossby waves.

This work is part of the author's PhD thesis completed in the Joint Program of MIT/Woods Hole Oceanographic Institution. The author would like to thank Dr J. Pedlosky for his advice and patient reading of previous manuscripts. Discussions with Dr G. Flierl are greatly appreciated. The author thanks S. Wijffels for her helpful suggestions and careful reading of the manuscript. The comments from two anonymous reviewers are appreciated. This work is supported by the Division of Atmospheric Research, NSF.

REFERENCES

ANDERSON, D. L. T. & KILLWORTH, P. D. 1979 Nonlinear propagation of long Rossby waves. *Deep-Sea Res.* **26**, 1033–1050.

CUSHMAN-ROISIN, B. 1984 On the maintenance of the Subtropical Front and its associated countercurrent. *J. Phys. Oceanogr.* **14**, 1179–1190.

DEWAR, W. 1987 Planetary shock wave. *J. Phys. Oceanogr.* **17**, 470–482.

HUA, B. L., MCWILLIMS, J. & OWENS, W. B. 1986 An objective analysis of the POLYMODE Local Dynamics Experiment. Part II: a streamfunction and potential vorticity fields during the intersive period. *J. Phys. Oeanogr.* **16**, 506–522.

LEVINE, E. R. & WHITE, W. B. 1981 Large-scale synoptic thermal fronts in the mid-latitude North Pacific from 1976–1978. *J. Geophys. Res.* **86**, 6567–6579.

LIU, Z. 1991 Time-dependent ventilated thermocline. PhD thesis, Joint Program of MIT/Woods Hole Oceanographic Institution.

LIU, Z. 1993*a* Penetration of interannual planetary waves across a gyre boundary. *Dyn. Atmos. Oceans* **17**, 169–186.

LIU, Z. 1993*b* Thermocline forced by varying Ekman pumping: I. Spin-up and spin-down. *J. Phys. Oceanogr.* (in press).

LIU, Z. 1993*c* Thermocline forced by varying Ekman pumping: II. Annual and decadal Ekman pumping. *J. Phys. Oceanogr.* (in press).

LUYTEN, J. R., PEDLOSKY, J. & STOMMEL, H. 1983 The ventilated thermocline. *J. Phys. Oceanogr.* **13**, 292–309.

MCWILLIAMS, J. C., BROWN, E. D., BRYDEN, H. L., EBBESMEYER, C. C., ELLIOTT, B. A., HEINMILLER, R. H., LIEN HUA, B., LEAMAN, K. D., LINDSTROM, E. J., LUYTEN, J., MCDOWELL, S. E., BRECKNER OWENS, W., PERKINS, H., PRICE, J. F., REGIER, L., RISER, S. C., ROSSBY, H. T., SANFORM, T. B., SHEN, C. Y., TAFT, B. A. & VAN LEER, J. C. 1983 The local dynamics of eddies in the western North Atlantic. In *Eddies in Marine Science* (ed. A. R. Robinson), pp. 92–113. Springer.

NIILER, P. P. & REYNOLDS, R. W. 1984 The three-dimensional circulation near the Eastern North Pacific Subtropical Front. *J. Phys. Oceanogr.* **14**, 217–230.

RHINES, P. B. 1986 Vorticity dynamics of the oceanic general circulation. *Ann. Rev. Fluid Mech.* **18**, 433–447.

RODEN, G. L. 1976 On the structure and prediction of oceanic fronts. *Nav. Res. Rev.* **29** (3), 18–35.

RODEN, G. L. 1980 On the subtropical frontal zone north of Hawaii During winter. *J. Phys. Oceanogr.* **10**, 342–362.

SCHOPF, P., ANDERSON, D. & SMITH, R. 1981 Beta-dispersion of low-frequency Rossby waves; *Dyn. Atmos. Oceans* **5**, 187–214.

TABARA, B., THOMAS, B. & RAMSDEN, D. 1986 Annual and interannual variability of steric sea level along line P in the Northeast Pacific Ocean. *J. Phys. Oceanogr.* **16**, 1378–1398.